Studying the Properties of Diffuse Atomic Halo Gas Surrounding the Milky Way and M83

Pallavi Maladkar

Contents

1 Introduction **1**

2 Background: Galactic Clouds **1**

3 Methods **2**
3.1 Data Collection 2
3.2 Extracting Data from Databases 2
3.3 Normalizing Fluxes 4
3.4 Calculating Equivalent Widths and Column Densities 5

4 Data Analysis **7**

5 Discussion **10**

6 Modeling **10**
6.1 Toy Model 10
6.2 Future Steps 12

Abstract

Diffuse atomic gas permeating and surrounding galaxies constitutes a large fraction of galactic baryonic mass. When these gas clouds are gravitationally accreted, they can interact with the interstellar medium and contribute significantly to the galactic star formation rate [6]. We focus on determining the spatial extent and kinematics of these gas structures along lines of sight to Messier 83. We employ absorption line spectroscopy and analyze 126 spectra of lines of sight oriented inside and surrounding Messier 83. We measure the absorption line strengths and calculate column densities of ionized Ca II gas observed around the Milky Way and Messier 83 along these lines of sight. We study the small scale variation in the density and masses of the gas clouds and observe several cloud structures orbiting Messier 83 and the Milky Way. We will present a preliminary model for the thickness and extent of the cloud assuming constant density. In the future, we look to extend this research to parameterize the accretion rate of the gas structures surrounding Messier 83 and the Milky Way.

1 Introduction

Galaxies are complex systems of gas, dust, and stellar material interacting to create the dynamic structures we see today. The way these components interact with one another is important to the kinematics and structure of galaxies. Using our knowledge of the individual components, we can piece together a picture of the larger scale processes.

When atomic gas clouds orbiting galaxies fall into the galactic disk due to gravitational effects, they can interact with the interstellar medium and contribute significantly to the star formation rate. Knowing the star formation rate of galaxies reveals the galaxy's history and evolution.

We attempt to detect these atomic gas clouds and observe their motion and structure in order to parameterize the rate at which gas accretes into galaxies, as well as understand how this affects the star formation rate. In this project, we will focus on detecting and observing the properties of diffuse atomic gas clouds orbiting the Milky Way and Messier 83. We will study the small scale variation in the density and masses of the gas clouds.

2 Background: Galactic Clouds

Absorption line measurements have established the presence of atomic gas above, below, and surrounding galaxies, including the Milky Way [5]. These large reservoirs of gas and metals are known as galactic halo clouds, difficult to detect because they emit and reflect little radiation and have low densities. There are two main classes of galactic halo clouds we will be concerned with in this paper: high velocity clouds (HVCs) and intermediate velocity clouds (IVCs) [6]. By deriving mass flow rates, we know that inflow and outflow of gas in galaxies is mainly driven by HVCs and their metallicities [3]. An artist's rendition of the position of HVCs and IVCs is shown in Figure 1.

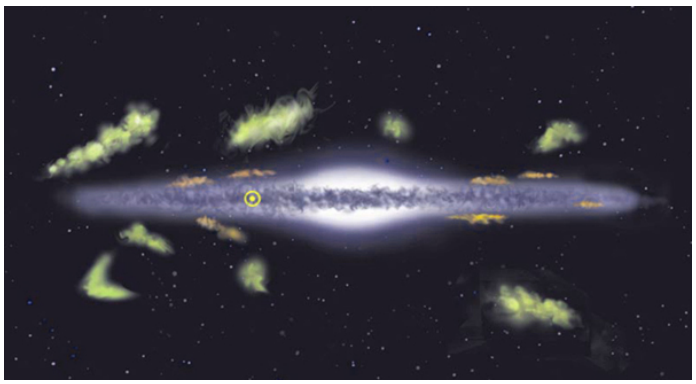

Figure 1: Schematic of galactic halo clouds orbiting spiral galaxy [4] HVCs are depicted in green above and below the galactic disk; IVCs are depicted in orange closer to the galactic disk. These structures will gravitationally accrete into the plane of the disk. If we assume similarity to the Milky Way, the thickness of the galactic plane is approximately 1000 light years, or 0.3 kpc, and the yellow dot would indicate the position of our sun.

The rate at which gas accretes into the galactic disk from galactic halo clouds can be represented by Equation (1) [6].

$$\frac{dM_{gas,disk}}{dt} = \eta \frac{M_{gas} v_{infall}}{d} \quad (1)$$

In this equation, η is the fueling parameter, which modulates the amount of infalling gas that accretes into the disk, M_{gas} is the total mass of the infalling gas, v_{infall} is the infall velocity of the gas, and d is the galactocentric distance. In Figure 1, the galactocentric distance is the approximate distance from a galactic halo cloud to the center of the bulge in the middle of the disk.

We attempt to observe these properties of gas structures to quantify the variables in Equation (1). We are able to determine properties of size, column density, and line of sight (LOS) velocity through atomic absorption spectroscopy. These properties will be later used to find the masses and other kinematic variables of the clouds.

3 Methods

3.1 Data Collection

The observations were obtained in service mode at the ESO Very Large Telescope (VLT) in Cerro Paranal, Chile during the spring semester of 2017. The targets were observed as a part of the program, "Mapping the Cool Circumgalactic Medium and Disk Interface of M83 with Calcium II" (099.A-0490(A), PI: Bordoloi). The program used the FLAMES/GIRAFFE spectrograph, a fiber-fed multiobject spectrograph mounted on the Nasmyth focus of UT2 (Pasquini et al. 2003). The GIRAFFE High Resolution Mode was used in the H395.8 setup (HR02), which allows access to the 385.4 and 404.9 nanometer wavelength range in the near-UV. The spectral resolving power, $\lambda/\delta\lambda$, was 22,700.

A total of 16 hours of integration were obtained. The raw scientific data was bias- and dark-subtracted, flat-fielded, and wavelength-calibrated using the instrument's pipeline v12.14.2 under the esorex environment. The source spectra were extracted in the SUM mode, and the individual exposures were summed up to improve the signal-to-noise ratio (S/N) of the extracted data.

In this project, we used information from the Flexible Image Transport System (FITS) files on the name of the pointing, its right ascension (RA), declination (DEC), wavelength values, flux values, and error on the flux values.

3.2 Extracting Data from Databases

We extracted the image of M83, as well as the spatial position of all pointings (lines of sight). These pointings are shown as blue dots in Figure 2.

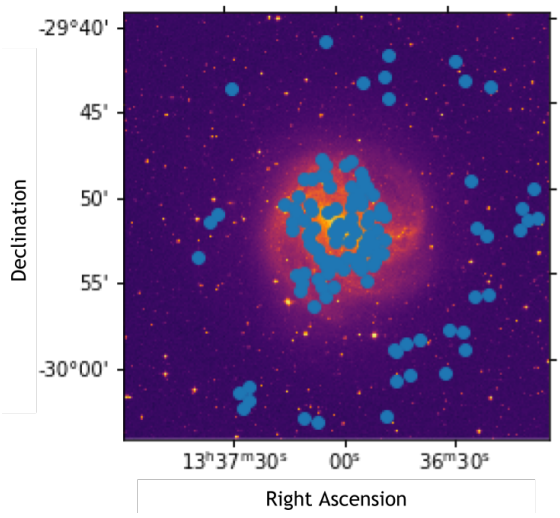

Figure 2: Pointings on M83 galaxy (Bordoloi) WCSMap, *false color image*

Our first step was to convert the wavelength values to LOS velocity values to account for redshift. We can also view the absorption signals in terms of velocities. Our function used two variables — the measured wavelength and the rest wavelength — and found a corresponding LOS velocity with Equation (2). We used two known rest wavelengths of Ca II, the H and K absorption lines, at 3968.4673 Å and 3933.6614 Å respectively.

$$v = (\lambda - \lambda_{rest}(1+z)) \cdot \frac{c}{\lambda_{rest}(1+z)} \tag{2}$$

Figure 3 shows the spectrum of the object with index 10, an object of interest because of its strong and distinct absorption signals. Object 10 is marked by the white cross on the right graph in Figure 3. We created 2 graphs, one plotting the LOS velocity values relative to the Milky Way's velocity and one plotting the LOS velocity values relative to M83's velocity, accounting for the redshift of M83 itself. Plotting the flux values relative to M83 shifts the spectrum from the Milky Way to the left by about 550 km/s, roughly the velocity of M83. This is done so that absorption signals of clouds orbiting M83 would appear closer to 0 km/s.

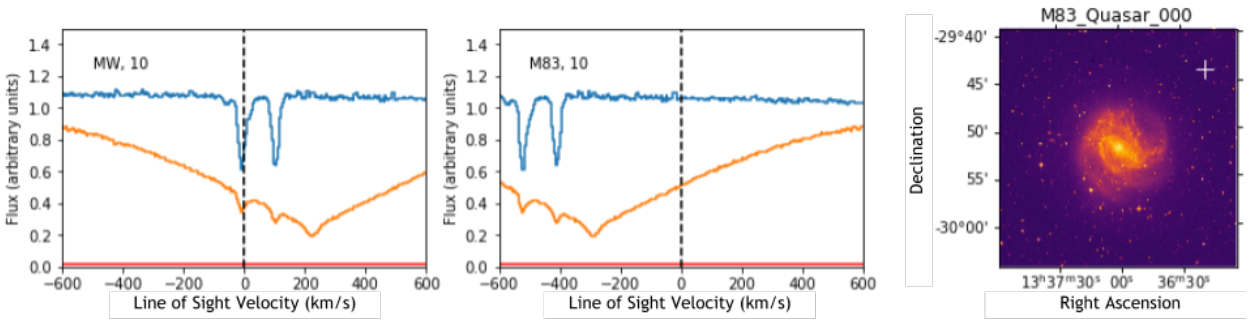

Figure 3: Spectrum and position of example line of sight corresponding to Pointing 10 Spectrum displayed corresponding to Ca II H absorption line (blue) and Ca II K absorption line (orange), with respect to Milky Way velocity (left) and M83 velocity (middle); position of Pointing 10 (right).

3.3 Normalizing Fluxes

All spectra have a characteristic fluctuation specific to individual pointings, caused by the continuum background noise from luminous objects. In order to accurately calculate the strength of absorption signals, this continuum must be normalized to 1.

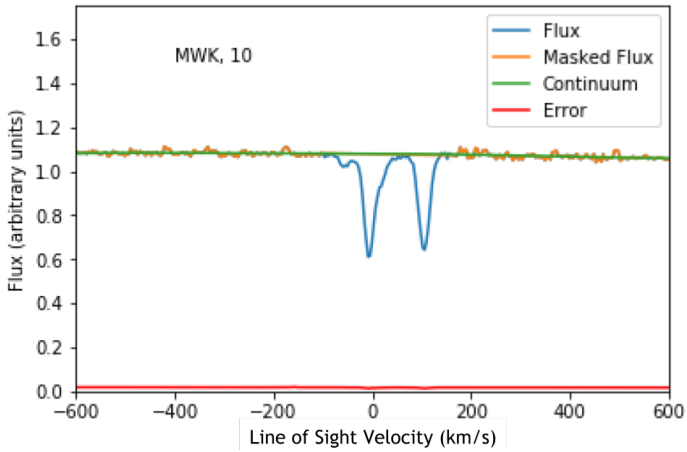

Figure 4: Fitting a continuum to a spectrum The blue curve represents the flux values. The yellow curve represents masked flux, or the flux values that exclude values that contribute to the absorption signals. The green curve is the polynomial fit, or continuum fit, to the masked flux. The red curve displays the error on the flux values at each corresponding LOS velocity. In this spectrum there is not much continuum fluctuation, so the fit appears to be nearly constant. In the top left corner of the graph, MWK indicates that we are considering velocities with respect to the Milky Way, and that we are using the K Ca II absorption line. 10 indicates we are considering the spectrum with index 10 (object 10).

We create a polynomial fit to the continuum. Before fitting the data, we cut out specific LOS velocity ranges containing the absorption signals. We then fit a polynomial of degree 5 to the continuum. We were able to manipulate the degree of the polynomial in order to create fits that matched the continuum accurately. This is shown for object 10 in Figure 4.

The next step would be to divide all flux values by the polynomial fit so the inherent fluctuations will be normalized to 1. The absorption signals, however, will be preserved. The result is the normalized flux, defined as $I_\lambda/I_{\lambda,0}$, in which I_λ represents the raw flux values and $I_{\lambda,0}$ represents the continuum of the flux. The normalized flux can also be represented by $e^{-\tau_\lambda}$, a function of optical depth. The normalized flux for object 10 is shown in Figure 5.

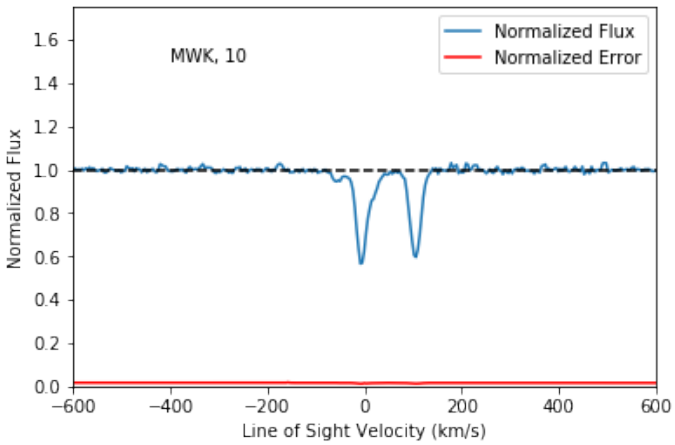

Figure 5: Normalized flux The blue curve represents the normalized flux, while the red curve represents the error on the flux divided by the same polynomial fit as the flux values. There is a dashed line at "normalized flux = 1", which makes it clear that the continuum has been normalized.

In Figure 5, we observe two prominent absorption signals. These correspond to two clouds moving at different velocities relative to us. The cloud with its signal centered around 0 km/s is moving at approximately 0 km/s relative to us. The other cloud that appears to have its absorption signal centered around 100 km/s is moving at approximately 100 km/s away from us. Using this method, we can begin analyzing the absorption signals of distinct clouds.

3.4 Calculating Equivalent Widths and Column Densities

We defined a function that takes in wavelength values, normalized flux values, rest wavelength, limits of integration, and normalized error values and calculates 4 things: the equivalent width and its corresponding error, and the column density and its corresponding error.

The equivalent width is defined as (M. Pettini: Physical Cosmology - Lecture 10):

$$W = \int_{-\infty}^{\infty} (1 - e^{-\tau_\lambda}) d\lambda \tag{3}$$

This equation calculates the area between the normalized flux values and the normalized continuum level, or where flux = 1. This is shown in Figure 6:

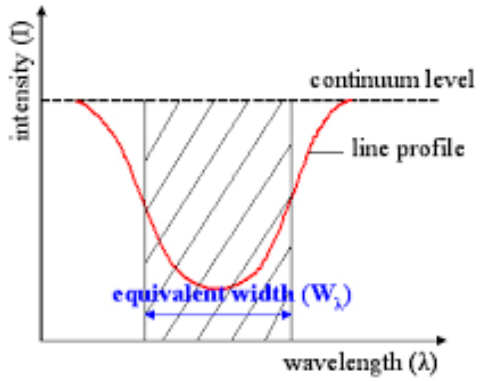

Figure 6: Definition of equivalent width [1] The red curve is representative of a spectrum with an absorption signal. The shaded region is a rectangle of height 1 (at the continuum level) and a width that gives the rectangle an area equal to the area between the line profile and the continuum level.

The column density is given by the following equation (M. Pettini: Physical Cosmology — Lecture 10):

$$N = 1.13 \times 10^{20} \cdot \frac{W_\lambda}{\lambda^2 f} \mathrm{cm}^{-2} \tag{4}$$

In this equation, W_λ is the equivalent width value at the specific wavelength in angstroms, λ is the wavelength value in angstroms, and f is the "oscillator strength", a dimensionless quantity that represents the probability of absorption or emission of electromagnetic radiation in transitions between energy levels of the atom or molecule [2].

For LOS velocities with respect to the Milky Way, integration limits (velocity ranges) were defined, and the equivalent width and column density was calculated for every spectrum using these limits. We repeated this process for various velocity ranges chosen by visually examining spectra for ranges containing the absorption signals.

For spectra with velocities with respect to M83, however, there was typically more broadening in the absorption signals. Defining a small range to integrate over would not have encompassed the true region of the absorption signal for all spectra. We created a table containing LOS velocity ranges defined specifically for the signal around 550 km/s in each spectrum. These velocity ranges covered any absorption lines centered around 0 km/s. The function used the values from the table for integration limits. It calculated the equivalent width and column density values, along with the error on those values, and stored them in the table.

Using these calculations, we can now analyze the data in numerous ways, whether it be spatially, observing trends between specific variables, etc. This analysis will be elucidated on in section 4.

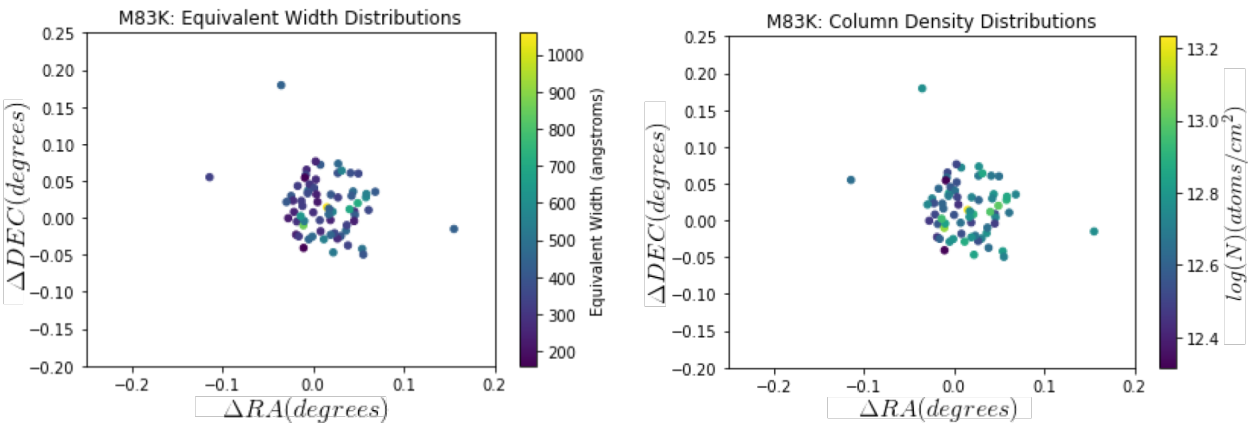

(a) Equivalent Width

(b) Column Density

Figure 7: M83 Equivalent width and column density distributions Graph a is color coded with respect to equivalent width distributions. Graph b is color coded with respect to column density distributions. However, in order to represent the column density values more accurately, we took the log of each column density value, so the color bar has a logarithmic scale.

4 Data Analysis

The first step in analyzing the data was to look at the spatial distribution of the pointings corresponding with our calculated values. We graphed the spatial distribution of the pointings on a coordinate plane, with axes of change in right ascension and declination, and color-coordinated the pointings based on equivalent width and column density. These are shown in Figure 7.

These graphs were created by integrating the normalized fluxes over ranges corresponding to clouds moving at around the speed of M83 (550 km/s). The graphs, then, show clouds orbiting M83.

If 3 times the value of the error on the equivalent width is more than the equivalent width value itself (EW $\leq 3\sigma$), the equivalent width for that pointing is deemed statistically insignificant. All such pointings are not plotted, which is why not all pointings appear on Figure 7a and 7b.

In analyzing these figures, we can discern specific cloud structures present based on spatial positioning of these absorption strengths. For example, at around 0 degrees RA and DEC, there seem to be many pointings coalesced into a central location, all with similar equivalent width and column density values (based on colors). This could indicate the presence of a gas cloud of roughly the extent of the colored pointings, with thicknesses over spatial positions corresponding with the column density measurements. The slight variation in column density values could be due to stronger or weaker concentrations in specific places, corresponding to smaller cloud structures, called cloudlets.

However, there does exist a bias in any conclusions we make. Many of the pointings are located in a central region covering M83, but we don't have an even distribution of pointings beyond its disk. If a gas cloud extended beyond the extent of M83, we could not discern its true size.

While in Figure 7, we indicate gas orbiting M83, we can also indicate gas orbiting the

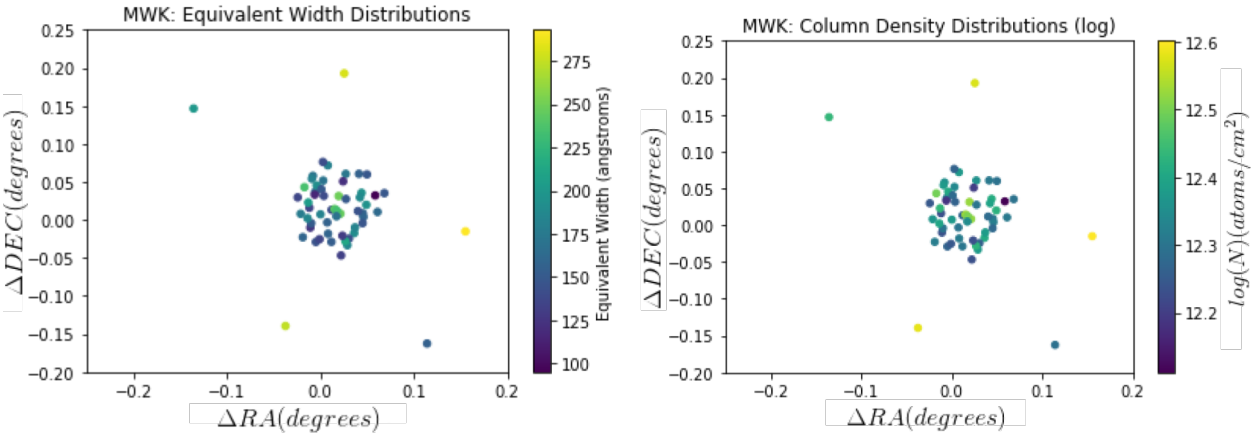

(a) Equivalent Width

(b) Column Density

Figure 8: Milky Way equivalent width and column density distributions Graph a is color coded with respect to equivalent width distributions. Graph b is color coded with respect to column density distributions. However, in order to represent the column density values more accurately, we took the logarithm of each column density value, so the color bar has a logarithmic scale.

Milky Way by integrating over velocities closer to 0 km/s. Figure 8 is graphed in a similar way as Figure 7, except we are now using column densities calculated by integrating over the LOS velocity range -90 to 40 km/s.

There are other ways to analyze the data we have collected in order to determine patterns and underlying structures. One of them involves comparing values of spatial distance and column density as angular separation increases from a specific point, such as the mean of all pointings. This is shown in Figure 9.

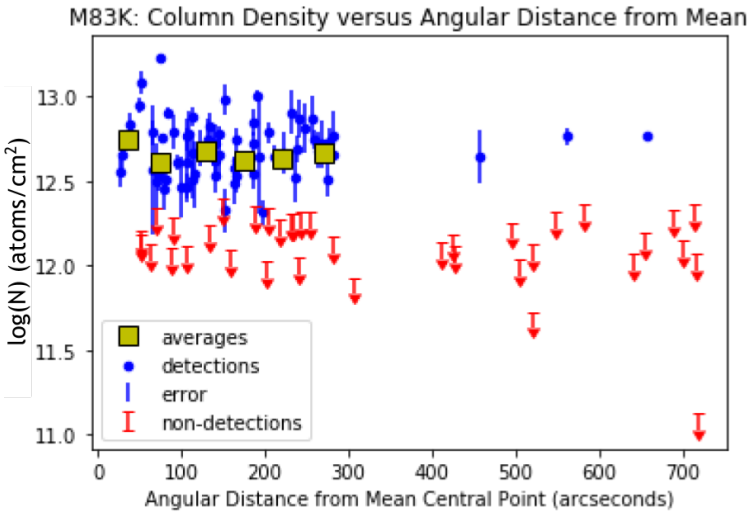

Figure 9: M83: column density variation with respect to mean central point We calculate the mean central point by averaging all RA and DEC values, and then calculate the angular distance from every pointing to the mean central point. All true detections are marked by blue points, with their corresponding error in blue error bars. All non-detections are marked by red arrows, with an upper bound at 2σ above the actual value. The column densities displayed in this graph represent a cloud orbiting M83.

The yellow boxes are calculated by averaging all the column density values in a certain range of arcseconds. For Figure 9, there are 6 ranges with widths of 50 arcseconds starting with 0 arcseconds. For the most part, all the average column density values for each range seem to be around the same value, indicating that the gas cloud has relatively uniform density extending outwards from the mean central point.

Another method of analyzing the data is to compare values of angular distance from a specific pointing to differences in column density in reference to that pointing's column density. A good example of one such pointing is object 10, which has a particularly strong absorption signal. We calculate the angular separation of each point from the coordinates of object 10. We plot this value in arcseconds on the x-axis. On the y-axis, we calculate the difference of each column density value from object 10's column density. This way, we can see the variance of column densities as distance increases from object 10. This is shown in Figure 10. We have calculated column densities by integrating over the range -90 to 40 km/s, which means that the column densities describe gas orbiting the Milky Way, most likely in the interstellar medium itself because of its proximity to 0 km/s.

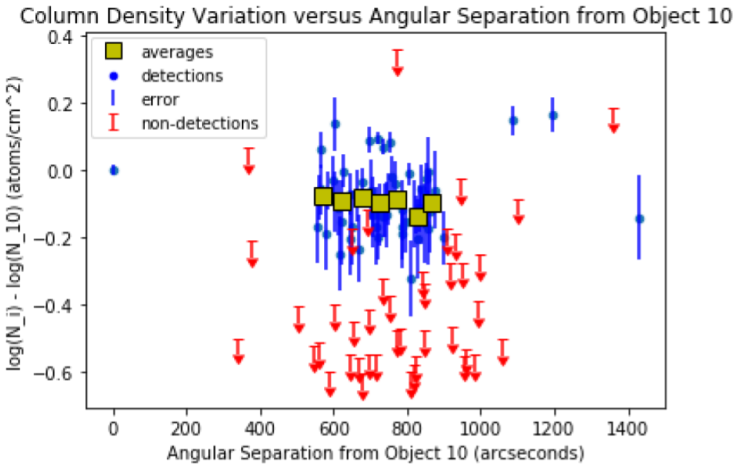

Figure 10: Milky Way: column density variation with respect to object 10 Blue dots represent column density difference values, vertical blue lines represent error on column density differences, red arrows indicate non-detections, with an upper bound at 2σ above the actual value of the reading. This graph displays information on a cloud orbiting the Milky Way.

The y-values of the yellow squares are found by taking the average of the column density values in a certain angular separation range — in this case 7 ranges each of size 50 arcseconds, starting at 550 arcseconds. By defining multiple ranges, we can calculate this "average value" over each range and observe a trend as distance increases from object 10. For example, in Figure 10, as distance increases from object 10, column density seems to be almost constant, deviating slightly. This could indicate that object 10 is at a point of higher atomic concentration in the gas cloud we are observing. As the gas cloud extends further, the concentration decreases slightly. This could also be explained by the presence of a dense cloudlet near object 10 moving at roughly 0 km/s away from earth.

5 Discussion

Through analysis of column density distributions over the range -90 to 40 km/s (Figure 8), we conclude the existence of a galactic halo cloud moving at around 0 km/s relative to Earth. Because of its low relative LOS velocity, it is most likely a cloud in the interstellar medium of the Milky Way or orbiting the Milky Way. Near M83's disk, there is a larger concentration of detections, with column densities at similar orders of magnitude. There are 5 detections outside M83's disk with varying column density strengths (seen in Figure 8b).

A possible solution is the existence of a large galactic cloud orbiting the Milky Way that has an extent beyond M83's disk. The slight variations in column densities across the region of M83's disk can be attributed to the existence of smaller cloudlets of gas, which add to the strength of signals. Cloudlets can also explain the 5 detections outside M83's disk as well.

In Figure 10, we suggest the detections are caused by the interstellar medium of the Milky Way, and possibly another cloud absorbing the Milky Way. We suggest this cloud is roughly uniform throughout, with slight deviations in the detections and the non-detections caused by the existence of cloudlets contributing to the column densities. It could be argued that object 10 is near the middle of a cloud with high density, while most of the surrounding pointings have lower densities. This implies that there is less gas as angular separation increases from object 10. However, this cannot be confirmed without knowledge of densities on all sides of object 10, and is weakened by the existence of 2 particularly strong detections at roughly 1100 and 1200 arcseconds. It could also be argued that object 10 is simply the location of a particularly dense or large cloudlet in the plane of the Milky Way.

We also analyzed column density distributions corresponding with atomic gas orbiting M83 (Figure 7), as M83 is moving at roughly 550 km/s away from us. Because most detections are located within M83's disk, we propose a galactic halo cloud roughly the size of the disk. Because we don't have many detections past the extent of M83's disk, we cannot accurately define the extent of this proposed cloud. Based on Figure 9, we know that the cloud orbiting M83 has roughly similar column densities throughout the extent of the detections. The number of non-detections (plotted in red) and the slight variances in the detections suggest the existence of cloudlets in the region as well.

6 Modeling

6.1 Toy Model

We will present a "toy model" using our calculated column densities. We assume all clouds are spheres of constant density and radius, and the pointings pass through clouds at various distances from the center of the sphere. This is shown in Figure 11.

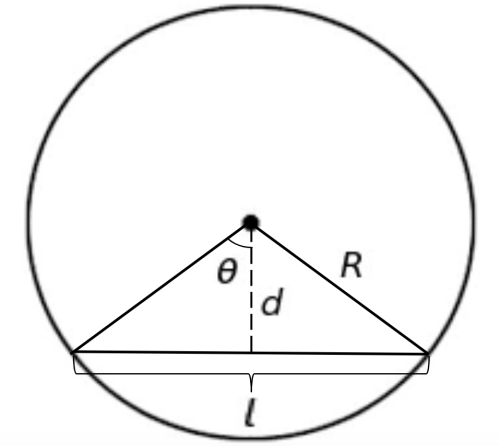

Figure 11: "Toy Model" Geometric representation of the toy model; R is the radius of the cloud, d is the impact parameter, or distance that we view the pointing to be from the center of the cloud, and l is the portion of the line of sight to the pointing that passes through the cloud.

Column density can physically be defined by the following equation:

$$N = \int \eta_0 dl = \eta_0 l \tag{5}$$

and using the geometry in Figure 11, can be represented by:

$$N = 2\eta_0 \sqrt{R^2 - d^2} \tag{6}$$

Using the relationship in equation (6), we can model the expected clouds by varying certain variables — radius of the cloud, impact parameter, and density of the cloud — to produce the calculated column densities.

We began by creating a list of random impact parameters (d in equation (6)), ranging from 0 to a maximum radius. We then created a function that took in the value for a density and a maximum radius, and used equation (6) to create a list of column density values with the density, radius, and list of random impact parameters. We then used the list of column density values and compared with our observed values from the spectra to find a χ^2 value using the following equation:

$$\chi^2 = \sum_{i=1}^{n} \left(\frac{N_i - N_{i(exp)}}{\sigma} \right)^2 \tag{7}$$

in which N_i is the observed column density, $N_{i(exp)}$ is the expected column density value, and σ is the standard deviation of the observed column density values. We then calculated the reduced χ^2 value with the following equation:

$$\tilde{\chi}^2 = \frac{\chi^2}{\nu} \tag{8}$$

in which ν represents the degree of freedom. $\nu = n - m$, where n is the number of observations and m is the number of fitted parameters. In our research, $n = 126$ and $m = 0$, so $\nu = n = 126$.

We used this function to attempt to minimize our reduced χ^2 value with various combinations of radii and densities. Figure 12 depicts some of the best combinations of radii and densities we considered.

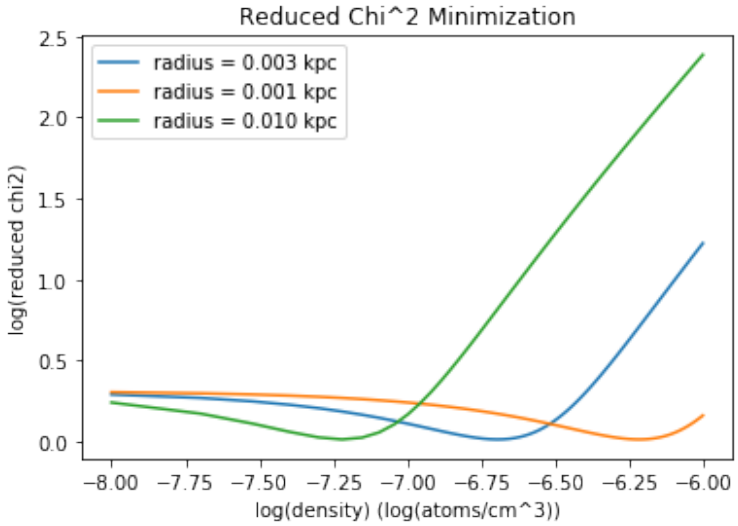

Figure 12: "Reduced χ^2 Minimization" We compare the log of density on the x-axis and the log of the reduced χ^2 values on the y-axis. Each line represents a different maximum radius.

We tried a variety of radius and density combinations: all combinations of radii and densities over the range 0 to 0.1 kpc (increments of 0.001 kpc) for cloudlet radius and 0 to $1 \cdot 10^{-6}$ atoms/cm^3 (increments of $1 \cdot 10^{-8}$ atoms/cm^3) for cloudlet density. We find that our reduced χ^2 value is minimized with a radius of $3 \cdot 10^{-3}$ kpc and a density of $2 \cdot 10^{-7}$ atoms/cm^3, represented by the blue curve in Figure 12. This should be the expected maximum radius and density of the observed cloudlets orbiting M83 according to our observations. Although a simple model, assuming all cloudlets have the same radius and density, it provides an idea of the relative sizes of these cloudlets.

Using this model for the approximate size and density of the cloudlets orbiting M83, we predict the mass of the Ca II gas in one of these cloudlets is $\approx 4.4 \cdot 10^{25}$ kg. Multiplying by the number of pointings with detections around M83 (69 significant detections), we obtain the total mass of gas orbiting M83 in Ca II, $\approx 3.1 \cdot 10^{27}$ kg. These calculations could be used in future approximations of cloudlet gas contribution to accretion in M83.

6.2 Future Steps

When examining column densities corresponding to clouds orbiting M83, subtracting out column density contributions from M83's interstellar medium would be a future step to better strengthen our model. Disregarding the contributions from the gas in the disk of the galaxy isolates the galactic structures orbiting the galaxy from our calculations. This can be done by using previous data on M83 interstellar medium absorption for the same pointings at which we found detections. We can then gain a more accurate understanding of the shape and distribution of the galactic halo clouds.

Acknowledgements

I would like to acknowledge Dr. Jonathan Bennett, my mentor and teacher at the North Carolina School of Science and Mathematics, for guiding me through the research process and ensuring that I thoroughly understand my project.
I would like to acknowledge Dr. Rongmon Bordoloi, my mentor and an assistant professor in the Physics Department at North Carolina State University, for his guidance and for providing me with the tools to conduct this research.
I would like to acknowledge Mr. Alvin Chen and my classmates in my Research in Physics class for supporting me and providing me with inspiration and useful advice throughout the research process.

References

[1] Equivalent width. Retrieved from https://en.wikipedia.org/wiki/Equivalent_width, May 2018.

[2] Oscillator strength. Retrieved from https://en.wikipedia.org/wiki/Oscillator_strength, Dec 2018.

[3] Andrew J. Fox, Philipp Richter, Trisha Ashley, Timothy M. Heckman, Nicolas Lehner, Jessica K. Werk, Rongmon Bordoloi, and Molly S. Peeples. The Mass Inflow and Outflow Rates of the Milky Way. *The Astrophysical Journal*, 884(1):53, Nov 2019.

[4] Ingrid Kallick. *Galactic Halo Clouds*. Scientific American, Jan 2004.

[5] N. Lehner, J. C. Howk, C. Thom, A. J. Fox, J. Tumlinson, T. M. Tripp, and J. D. Meiring. High-velocity clouds as streams of ionized and neutral gas in the halo of the Milky Way. *Monthly Notices of the Royal Astronomical Society*, 424(4):2896–2913, Oct 2012.

[6] Philipp Richter. Gas Accretion onto the Milky Way. *Astrophysics and Space Science Library*, 430:15–47, Jan 2017.